Longitudinal Blood Immune-Inflammatory and Radiomic Profiling to Decode Different Patterns of Acquired Resistance to Immunotherapy in Patients with NSCLC

Giulia Mazzaschi[1,2], Cristina Marrocchio[2,3], Lucas Moron Dalla Tor[2], Ludovica Leo[2], Maurizio Balbi[4], Gianluca Milanese[2,3], Ganiyat A. R. Adebanjo[2,3], Bruno Lorusso[2], Gregorio Monica[5], Monica Pluchino[1], Roberta Minari[1], Simona D'Agnelli[1], Elisa Cardinale[1,2], Fabiana Perrone[1], Paola Bordi[1], Alessandro Leonetti[1], Roberta E. Ledda[2,3], Mario Silva[2,3], Sebastiano Buti[1,2], Giovanni Roti[2,5,6], Stefano Bettati[2], Federico Quaini[2], Marcello Tiseo[1,2], and Nicola Sverzellati[2,3]

ABSTRACT

Purpose: To uncover the underpinnings of acquired resistance (AR) to immunotherapy (IO), we determined whether distinctive clinicopathologic, radiomic, and peripheral blood (PB) immune-inflammatory features reflect oligo- and systemic (sys)-AR in patients with advanced non–small cell lung cancer (NSCLC) undergoing immune checkpoint inhibitor therapy.

Experimental Design: On 105 consecutive patients with IO-treated advanced NSCLC, PB immunophenotypes, cytokines, and CT-derived radiomic features (RF), extracted from primary and merged metastatic lesions, were prospectively collected at baseline (T0) and at the first disease assessment (T1, 9–12 weeks), and their Δ variation [(T1−T0)/T0] was computed. AR, defined as progression after the initial response (complete/partial) or stable disease ≥6 months, was subdivided according to the number of new and/or progressive lesions in oligoAR (≤3) and sysAR (>3). Clinicopathologic, PB, and radiomic parameters and survival outcomes were statistically correlated to AR patterns.

Results: OligoAR and sysAR involved 24% and 12.4% of cases, respectively. Whereas baseline PB immune profiles were comparable, a Δ^{pos} cytotoxic (NK, $CD8^+$granzyme B^+) and Δ^{neg} immunosuppressive ($CD14^+$ monocytes) dynamic coupled with different modulations of IL-6, TGF-β1, TNFα, and soluble PD-L1 represented distinctive features of oligoAR versus sysAR ($P < 0.05$). Significantly longer postprogression survival characterized oligoAR versus sysAR (median 20.3 vs. 5.6 months; HR, 0.22; $P < 0.001$). The number and sites of oligoAR involvement appeared to condition the blood immune background ($P < 0.05$) and survival. ΔRFs outperformed baseline RFs, with 15 ΔRFs sharply discriminating oligoAR from sysAR (P range: <0.001–0.04). ROC analysis confirmed the optimal performance of top-ranked ΔRFs (AUC range: 0.88–0.99).

Conclusions: Longitudinal analysis of blood-immune hallmarks and radiomic descriptors may decipher distinct patterns of AR to IO in advanced patients with NSCLC.

Introduction

The turning point in cancer treatment set by the advent of newly discovered PD-(L)1 immune checkpoint–targeting agents soon uncovered a heterogenous path of response (1). Specifically, the response rate to immunotherapy (IO)-based regimens has been variably assessed according to different tumor contexts, albeit never exceeding, under the best circumstances, 45% to 50% of cases (2).

Biomarkers of IO efficacy, such as PD-L1 expression (3), tumor mutational burden (4), HLA genotype (5), and additional tumor genomic [i.e., microsatellite instability (6)] and microenvironmental [i.e., tumor-infiltrating lymphocytes (7, 8)] features, still leave uncovered the underpinnings of the mixed clinical response to IO. Whereas these studies largely involving patients with non-small cell lung cancer (NSCLC) and melanoma have significantly improved our knowledge of how the immune system can be harnessed to kill cancer cells, the multi-level biological and clinical heterogeneity imposes to redesign our current strategy to expand the population of patients with cancer who can benefit from such a powerful therapeutic tool (9).

Discrepancy in tumor regression among primary and secondary diseases as well as within different metastatic sites is frequently reported (9, 10). Atypical patterns, like pseudoprogressive disease, hyperprogressive disease, and dissociated response, are clearly recognized in patients with NSCLC undergoing IO (10–12).

Primary resistance consists of a lack of an upfront response to IO, whereas adaptive resistance reflects cancer tuning to the immune attack (1, 13). Acquired resistance (AR) refers to a radiologic and/or clinical progression of the disease following an initial response to IO. A threshold of three new or progressive lesions (PL) has been proposed in large series of patients with metastatic lung cancer to distinguish oligoAR from systemic AR (sysAR), respectively (14, 15). Longer postprogression survival

[1]Medical Oncology Unit, University Hospital of Parma, Parma, Italy. [2]Department of Medicine and Surgery, University of Parma, Parma, Italy. [3]Radiological Science Unit, University Hospital of Parma, Parma, Italy. [4]Radiology Unit, University of Turin, Turin, Italy. [5]Translational Hematology and Chemogenomics, University of Parma, Parma, Italy. [6]Hematology and BMT Unit, University Hospital of Parma, Parma, Italy.

G. Mazzaschi and C. Marrocchio contributed equally as first authors to this article.

M. Tiseo and N. Sverzellati share co-last authorship to this article.

Corresponding Author: Giulia Mazzaschi, Department of Medicine and Surgery, University of Parma, via Gramsci 14, Parma 43126, Italy. E-mail: giulia.mazzaschi@unipr.it

Clin Cancer Res 2025;XX:XX–XX

doi: 10.1158/1078-0432.CCR-24-1926

Translational Relevance

Despite the groundbreaking success of immunotherapy (IO), nearly half of IO-treated patients with NSCLC develop acquired resistance (AR), strengthening the need to unveil the immunobiologic underpinnings of this common event. Further AR-related pitfalls reside in the variable clinical appearance enclosing the so-called oligo- and systemic-AR according to the extent of involved sites. Decoding the heterogeneity of tumor–host interactions underlying AR is critical to timely introduce treatment changes expanding the population of IO-responsive patients. Herein, we show that longitudinal monitoring (i.e., up to 12 weeks) of radio-immune profiles may capture lesion-level response dynamic, thus early-identifying the occurrence of AR patterns in patients with advanced NSCLC undergoing IO. Specifically, Δ radiomic features and the balanced output of blood immune-effector and immune-suppressor cells, along with a differential cytokine modulation, sharply discriminate oligo- from systemic-AR patients. Noninvasive approaches tracking AR onset and evolution may represent a translatable tool to guide clinical decision-making in IO-treated NSCLC.

was observed in oligoAR compared with sysAR cases, suggesting that under this setting, a restoration of the initial durable response to IO can be achieved following local therapy (15). AR is regarded as a heterogeneous condition owing to multiple tumor- and host-related features (16, 17), and the impact of organ- and/or tissue-specific immunity, so-called immunostat (18), on this pattern of response has been recently proposed.

Single-cell analysis strongly favors the peripheral origin of tumor-specific T-cell clones implicated in IO response (19, 20), suggesting blood as an easily accessible source to intercept critical factors involved in the cancer-immunity cycle and its perturbation following IO. Moreover, the capacity to noninvasively capture lung cancer phenotypic characteristics can be exploited by the application of radiomics. Recent studies have shown how radiomic features (RF) can be processed in an artificial intelligence (AI) fashion for patient risk stratification and prediction of clinical outcomes in the setting of IO (21–23), including potential application to the assessment of lesion-level response (24, 25). Thus, blood sampling and radiologic imaging may allow timely monitoring imposed by the dynamic nature of tumor–host interaction during IO administration.

The purpose of the present study was to determine whether distinctive clinicopathologic, radiomic, and circulating immune-inflammatory features discriminate oligoAR from sysAR in patients with IO-treated NSCLC, thereby conditioning different survival outcomes and therapeutic efficacy.

Materials and Methods

Patients and clinical samples

The outline of this prospective observational study (AIRC IG ID. 23606) is illustrated in **Fig. 1A**. The present cohort included patients with metastatic NSCLC who underwent systemic IO treatment as first- (IO alone or combined with platinum-based chemotherapy) or second-line of treatment at the Medical Oncology Unit of the University Hospital of Parma from November 2020 to June 2023 (database lock on December 2023).

The main inclusion and exclusion criteria are reported in Supplementary Materials and Methods. Briefly, patients with stage IV disease who were not susceptible to curative therapy, eligible for IO, and not previously treated with IO were included, whereas cases with active pneumonitis, unavailable clinical, tissue, blood, or imaging data, and prior immunotherapy were excluded.

The study was approved by the Ethics Committee (229/2020/OSS/UNIPR) and was therefore conducted in accordance with the ethical principles derived from the Declaration of Helsinki. Written informed consent was obtained from all investigated patients. Patient characteristics were extracted from medical and pathology records.

Clinicopathologic parameters (i.e., sex, age, performance status, concomitant medications, type of treatment, histology, and disease burden), blood samples, and CT images were appraised before starting immune checkpoint inhibitor therapy (T0) and at first radiologic reassessment after 9 to 12 weeks (T1).

Patients with inadequate follow-up (<6 months) were excluded from the subsequent analyses.

Definition of different patterns of response to IO

Three cohorts of patients developing distinct patterns of IO response were analyzed:

- AR group: AR to IO-based treatment was defined as disease progression after any initial objective response, either partial response (PR) or complete response (CR), or stable disease (SD) for ≥6 months according to RECIST criteria version 1.1. AR was further categorized into oligoAR and sysAR according to the number of new and/or progressive lesions of disease (oligoAR ≤3 new or progressive lesions; sysAR >3 new or progressive lesions; ref. 15).
- Nonresponder (NR) group: patients who experienced disease progression or SD <6 months as the best response (RECIST 1.1).
- Long-term/nonprogressor (LT-NP) group: patients who displayed progression-free survival (PFS) lasting more than 12 months or did not experience progression after a minimum follow-up of 12 months.

Peripheral blood analysis

Peripheral blood (PB) samples (10–12 mL) were analyzed to determine multiple parameters by different methodologic procedures. Time/treatment-dependent changes in PB variables were expressed as a percentage of Δ variation, $\Delta\ \% = [(\text{T1 value} - \text{T0 value})/\text{T0 value}] \times 100$.

Flow cytometric analysis

EDTA blood samples were analyzed by FACS (to assess the percentage and absolute number of $CD3^+$, $CD4^+$, and $CD8^+$ T cells, $CD3^-CD56^+CD16^+$ NK cells, $CD19^+$ B lymphocytes, $CD14^+$ monocytes, and $CD4^+CD25^+CD45RA^-FOXP3^{high}$ regulatory T cells (Treg). The expression of PD-1, granzyme B (GnzB), perforin, and Ki67 was also examined. The methodology, gating strategy, and the list of antibodies were previously reported (26) and are detailed in Supplementary Materials and Methods; Supplementary Fig. S1; Supplementary Table S1.

Soluble PD-L1 and cytokines

The levels of soluble PD-L1 and cytokine network (IL-1β, IL-2, IL-4, IL-6, IL-10, IL-12p70, IFNγ, TNFα, and TGF-β1) were

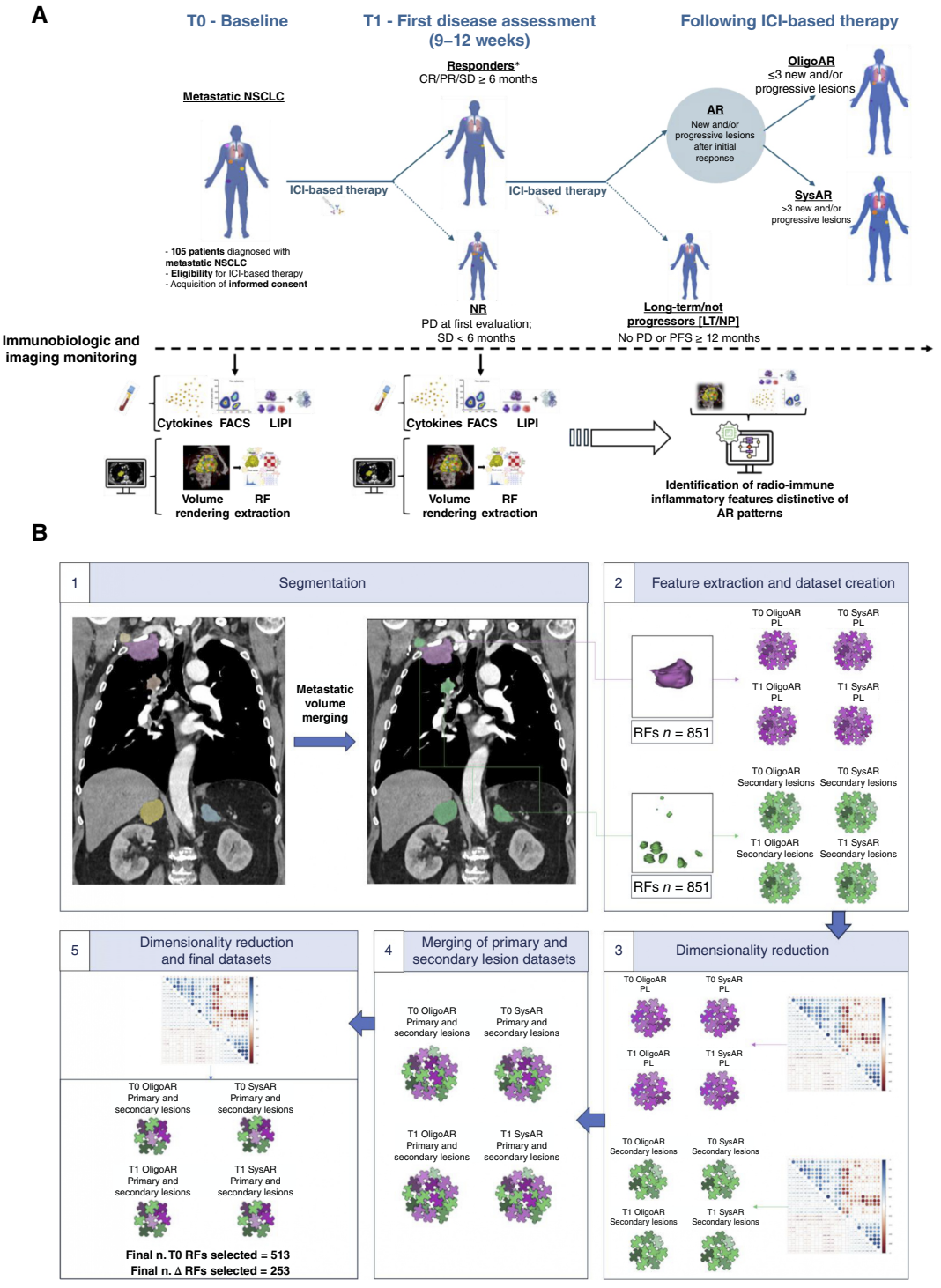

Figure 1.

Study design and radiomic workflow. **A,** Schematic representation of the study design reporting the included population and the workflow for the multiscale investigation. **B,** Radiomic approach illustrating lesion segmentations, dataset creation, and preprocessing to select the final number of RFs. *, For patients with SD, the stratification in responders vs. NRs was computed at the second radiologic disease assessment (6 months). **A,** Image created in BioRender. Mazzaschi, G. (2024) https://app.biorender.com/illustrations/65b7c316cc151905ea2bc308. ICI: immune checkpoint inhibitor; PD: progressive disease; SD: stable disease.

measured by ELISA immunoassay (multianalyte custom Plex Assay panel for Ella platform, Bio-Techne) on 200 μL of plasma.

Lung immune prognostic index score

Neutrophil to lymphocyte ratio (NLR) and derived NLR [absolute neutrophil count/(white blood cell concentration − absolute neutrophil count)] were manually computed. Lung immune prognostic index (LIPI) score was calculated based on derived NLR and lactate dehydrogenase levels according to published criteria (27).

Lactate dehydrogenase, hemocytometric, and LIPI measurements are further described in Supplementary Materials and Methods.

CT imaging and radiomic analysis

Image acquisition and segmentation

CT images at T0 and T1 were acquired using various CT scanners, including SOMATOM Definition Edge, Emotion 16, and SOMATOM go.Top (Siemens Healthineers). The technical parameters of image acquisition are summarized in Supplementary Table S2. The radiomic analysis was carried out on patients with AR, and to enable a systematic assessment of the disease, only subjects with available CT scans at both time points and having both the primary tumor and secondary lesions were considered. Contrast-enhanced CTs were selected for semi-automatic segmentation of pulmonary lesions with an open-source software (3D Slicer, version 5.6.1, RRID: SCR_005619). Segmentation was performed by a thoracic radiologist with 4 years of experience who was blinded to clinical data. Selection criteria for segmented lesions are described in Supplementary Materials and Methods.

RF extraction and analysis

RFs were extracted separately from the primary tumor and from the secondary lesions, the latter merged into a unique volume before feature extraction. To counter different slice thicknesses, volumes of interest were resampled to $1 \times 1 \times 1$ mm voxel size using linear interpolation. Signal intensity values were discretized to a bin width of 25 to further reduce variability. The open-source extension plugin PyRadiomics (version 3.1.0, RRID: SCR_026019), available on 3D Slicer software, was used for extracting data. Eight datasets were generated from extracted RFs based on the type of AR, CT time point, volume of origin, and whether the patient underwent postprocessing. Spearman correlation was computed for each dataset, and for each pair of features with absolute correlation ≥0.99, only one was retained. The primary lesion datasets ("P"-labeled RFs) and the metastatic lesion datasets ("M" RFs) were merged to obtain integrated data for both volumes. A Spearman correlation was then recomputed to remove redundant features across the two volumes, as described above (**Fig. 1B**).

T0 RFs selected after preprocessing that were common to oligoAR and sysAR were compared to assess the differences between the two populations. When considering both time points, postprocessed RFs common to T0 and T1 in oligoAR cases and RFs common to T0 and T1 in sysAR cases were identified. The Δ variation for oligoAR and sysAR datasets was computed using the following formula: $\Delta = (T1-T0/T0)$.

Statistical analysis

As IO outcome measures, we considered overall survival (OS), calculated from the date the patient began treatment to the date of death or the last follow-up; PFS, calculated from the date of treatment start to the date of clinical or radiologic progression or death or the last follow-up; postprogression OS, defined from the date of progression on IO to death or the last follow-up; modified disease control rate, defined as PR/CR or SD lasting ≥6 months; and objective response rate, defined as the proportion of patients with CR or PR.

Follow-up and survival times were estimated according to the Kaplan–Meier method. To assess statistical differences in PFS and OS between groups, we used the log-rank test (Mantel–Cox). The PFS and OS data were subsequently analyzed through Cox regression proportional hazards models, and the results were expressed as HRs, 95% confidence interval (CI), and *P* values.

Categorical and continuous variables were summarized using descriptive statistics. Fisher exact test or $\chi 2$ were used to examine differences between categorical variables, whereas Wilcoxon (nonindependent data), Mann–Whitney (independent data), or Kruskal–Wallis tests were used to detect differences in continuous variables between patient groups, as the distribution of data was not normal (Kolmogorov test by Smirnov). For radiomic data, principal component (PCA) analysis was carried out to assess the potential impact of CT technical parameters on RFs. To strengthen the results obtained from comparing RFs between patients' groups, in addition to the Mann–Whitney test, a permutation test based on median difference (with 1,000 permutations), was performed. Features were defined as meaningfully different when resulting significant at both Mann–Whitney and permutation tests.

The performance of statistically significant features was tested using the ROC curve analysis and the ROC-AUC score.

The *P* value of 0.05 was set as the threshold of statistical significance. Statistical analyses were performed with Jamovi software version 2.3 (www.jamovi.org, RRID: SCR_016142), R software (version 4.3.2), its ggplot2 package (RRID: SCR_014601), and GraphPad Prism software version 7 (www.graphpad.com, RRID: SCR_002798).

Data availability

Data are not publicly available due to patient privacy concerns. The data generated in this study are available upon reasonable request from the corresponding author.

Results

Patient population

A total of 105 patients (median age 68 years, 65% male) with stage IV NSCLC constituted the study cohort. Most patients were smokers, either former (47%) or current (41%). Adenocarcinoma was diagnosed in 76% of cases, and specific molecular alterations were identified in 45 patients (*KRAS*, $n = 40$; $EGFR^{exon20}$, $n = 3$; $BRAF^{V600E}$, $n = 2$; Supplementary Table S3).

The representativeness of study participants is shown in Supplementary Table S4.

The IHC expression of PD-L1, as assessed by the tumor proportion score on 94% of cases, resulted <1% in 22 (21%), 1% to 49% in 52 (49%), and ≥50% in 25 (24%) samples.

In 40 patients, less than three metastatic sites were involved, whereas the remaining 65 patients had three or more secondary disease localizations. The most affected organs were lymph nodes (83%), lung (72%), bone (35%), pleura (28%), brain (27%), adrenal gland (16%), and liver (11%). IO was administered as first-line therapy in 85 (81%) patients, combined with platinum-based chemotherapy (chemotherapy + immune checkpoint inhibitors) in

71 cases (83%), and administered as monotherapy in 34 cases with a predominant use of pembrolizumab.

At a median follow-up of 27.2 months (95% CI, 23.8–29.2), median PFS and OS were 7.1 months (95% CI, 5.7–10.2) and 16.5 months (95% CI, 12.0–26.3), respectively. The modified disease control rate) resulted 65%, whereas the objective response rate was 50% (Supplementary Fig. S2).

Of 105 patients with NSCLC, 70 had an initial response to IO (PR/CR) or SD ≥6 months, among which 26 did not experience disease progression, whereas 44 patients (63% of initial responders) met the definition of AR and were further analyzed for the patterns of resistance. Within this cohort, 26/44 (59%) cases displayed oligoAR features, whereas 18/44 (41%) belonged to sysAR (Supplementary Fig. S2).

The median time from starting IO to AR onset was 8.9 months (range: 6.2–18.7), with sysAR developing at a shorter pace (median: 7.7 months vs. 12.3 months in oligoAR cases; $P = 0.09$).

AR

Clinicopathologic characteristics

As shown in **Table 1**, the distribution of baseline clinical characteristics and tumor histotype among patients who developed oligoAR did not substantially differ from that of sysAR and LT-NP cases, except for liver metastatic involvement which was absent in oligoAR but affected 22% of sysAR patients. Compared with oligoAR, NR cases tended to exhibit a higher number of metastatic sites ($P < 0.05$) and higher intake of steroids before IO ($P < 0.05$). No differences were observed in tumor PD-L1 expression between oligoAR and sysAR, whereas a trend toward a higher frequency of cases with tumor proportion score ≥50% was noted in the LT-NP group (**Table 1**).

PB immune-inflammatory features

We initially investigated whether the circulating immune-inflammatory profile of the population of patients with NSCLC exhibiting AR differed from that of LT-NP and NR groups. At baseline, PB from LT-NP was characterized by a higher absolute number of lymphocytes ($P = 0.05$) and a trend toward higher $CD8^+GnzB^+$ cells, whereas NRs tended to display higher $CD14^+$ monocytes also expressing PD-1. An intermediate magnitude between LT-NP and NR of these circulating immunophenotypes was apparent in AR (Supplementary Fig. S3). Moreover, the fraction of patients with poor LIPI was significantly higher in NRs ($P = 0.015$), whereas good LIPI was equally distributed among AR and LT-NP patients.

At T1, we observed the lowest number of lymphocytes ($P = 0.006$) and a trend toward the lowest NK^{dim} and greatest fraction of $CD14^+PD\text{-}1^+$ monocytes in NRs. Conversely, LT-NP cases exhibited the highest rise (Δ+) of $CD8^+perforin^+$ ($P = 0.04$) and NK ($P = 0.03$) cytotoxic cells (Supplementary Fig. S3). AR patients largely displayed an intermediate extent and kinetic of these cytotoxic and immunosuppressive cells as a midway distribution of the LIPI score, with the highest fraction of poor LIPI scores belonging to NR cases and the highest fraction of good LIPI scores to LT-NP cases ($P = 0.010$).

OligoAR and sysAR

Baseline immune-inflammatory features and RFs

Baseline PB immune cells and cytokines were not significantly different between oligoAR and sysAR (Supplementary Table S5), except for higher baseline values of TGF-β1 ($P < 0.05$) and a trend toward increased IL-6 in sysAR (**Fig. 2**).

For RFs, the scatterplots obtained from the PCA of the CT technical parameters for both T0 and T1 timepoints are shown in Supplementary Fig. S4. Differently from immune-inflammatory data, radiomic analysis carried out on 12 oligoAR and 7 sysAR cases who had retrievable CTs and concomitant primary tumor and metastatic lesions at both time points revealed distinctive baseline RFs. Of 513 RFs selected after removing highly correlated features, 7 (one from the primary lesion and six from the metastatic volume) showed a statistically significant difference between the two AR subsets at T0 (P values range at Mann–Whitney test: 0.005–0.04; P values range at permutation test: 0.005–0.05; Supplementary Fig. S5).

Δ Immune-inflammatory features and RFs

Specific immune-inflammatory profiles emerged at T1, with oligoAR patients exhibiting a higher number of lymphocytes involving T (CD4 and CD8) and $CD19^+$ B ($P < 0.05$) cells compared with sysAR. We also documented a positive Δ variation of absolute lymphocyte count, $CD8^+$ subset, and NK cells in oligoAR as opposed to a decline in sysAR ($P < 0.05$; **Fig. 2A**). Additionally, a greater rise in cytotoxic ($GnzB^+$) and proliferative ($Ki67^+$) properties of CD8 ($P = 0.05$) ensued during IO in oligoAR compared with sysAR together with an increased percentage of cycling $CD4^+$ lymphocytes ($P = 0.05$). PB from sysAR was further characterized by an on-treatment rise (Δ+) in immunosuppressive $CD14^+$ cells, at variance from oligoAR in which this population tended to decline (**Fig. 2A**).

The dynamic analysis of the plasma cytokine array during IO showed a striking downregulation of TGF-β1 in sysAR ($P < 0.05$), reaching levels comparable with oligoAR at T1. IL-6 was inhibited as well, although persistently higher ($P < 0.05$) in sysAR versus oligoAR. Increased soluble PD-L1 ($P < 0.05$) levels characterized sysAR at T1, and TNFα and IFNγ values tended to display a greater increase in sysAR at T1, although not reaching statistical significance (**Fig. 2B**). The results on IL-1β, IL-2, IL-12p70, IL-10, and IL-4 did not allow a reliable evaluation due to the evidence that most measured amounts were near the range of sensitivity.

Following feature preprocessing and dimensionality reduction, 253 Δ RFs from the selected 12 oligoAR and 7 sysAR cases were analyzed. Fifteen Δ RFs were remarkably different between oligoAR and sysAR groups (P values range at Mann–Whitney test: <0.001–0.04; P values range at permutation test: 0.007–0.05; **Fig. 2C**), of which five derived from the merged metastatic volume and ten from the primary lesion. No shape feature was identified as statistically different. A detailed comparison of significant Δ RFs between oligoAR and sysAR is shown in **Table 2**; Supplementary Fig. S6. The ROC analyses documented a very good performance of significant Δ features in discriminating AR patterns. The six most different Δ RFs between the two populations (P value ≤0.007 at ROC analysis) showed AUC values ranging from 0.88 to 0.99, with P values ranging from 0.007 to 0.001 (**Fig. 2D**; **Table 2**). All these features were extracted from the primary lesions and included both first-order statistics and higher-level features.

Postprogression survival outcome and management

Patient outcomes after the occurrence of IO resistance significantly diverged between oligoAR and sysAR. Despite similar

Table 1. Baseline clinicopathologic characteristics according to IO outcome.

	OligoAR	SysAR	LT-NP	NR
	(*n* = 26)	(*n* = 18)	(*n* = 26)	(*n* = 35)
Age, years median (range)	68 (41–81)	68 (54–85)	69 (46–83)	71 (55–89)
	n (%)			
Histotype				
SCC	6 (23)	3 (17)	3 (12)	4 (11)
ADC	19 (73)	14 (78)	20 (77)	27 (77)
NSCLC NOS	1 (4)	1 (6)	3 (12)	4 (11)
Sex				
Male	16 (62)	9 (50)	16 (62)	27 (77)
Female	10 (40)	9 (50)	10 (39)	8 (23)
Smoking status				
Smokers	11 (42)	8 (44)	13 (50)	11 (31)
Ex-smokers	12 (46)	6 (33)	10 (39)	21 (60)
Nonsmokers	3 (12)	3 (17)	3 (12)	3 (9)
ECOG PS				
0–1	25 (96)	16 (89)	26 (100)	29 (83)
2	1 (4)	2 (11)	0	6 (17)
Steroids before IO				
Yes	3 (12)	3 (17)	4 (15)	12 (34)
No	22 (85)	14 (78)	22 (85)	22 (63)
Antibiotics before IO				
Yes	0 (0)	0 (0)	3 (12)	31 (89)
No	26 (100)	17 (94)	22 (85)	4 (11)
PPI before IO				
Yes	11 (42)	10 (56)	8 (31)	20 (57)
No	15 (58)	8 (44)	18 (69)	14 (40)
Number of metastatic sites				
<3	9 (35)	9 (50)	14 (54)	8 (23)
≥3	17 (65)	9 (50)	12 (46)	27 (77)
Metastatic involvement				
Bone	8 (31)	4 (22)	7 (27)	18 (51)
Brain	7 (27)	4 (22)	9 (35)	8 (23)
Liver	—	4 (22)	1 (4)	6 (17)
Lung	21 (80)	14 (78)	12 (46)	29 (83)
Lymph nodes	23 (89)	15 (83)	19 (73)	30 (86)
Adrenal gland	1 (4)	4 (22)	5 (19)	7 (20)
Pleura	8 (31)	7 (39)	3 (12)	11 (31)
Treatment type				
Single-agent IO	7 (27)	5 (28)	10 (38)	12 (34)
Chemotherapy–IO	19 (73)	13 (72)	16 (62)	23 (66)
Treatment line				
First	23 (89)	15 (83)	24 (92)	23 (66)
Second	3 (11)	3 (17)	2 (8)	12 (34)
PD-L1 status				
TPS ≥50%	5 (19)	3 (17)	11 (42)	6 (17)
TPS 10%–49%	4 (15)	1 (6)	2 (4)	5 (14)
TPS 1%–10%	11 (42)	8 (44)	9 (35)	13 (37)
TPS <1%	4 (15)	4 (22)	4 (15)	10 (29)
Unknown	2 (8)	2 (11)	1 (4)	—
Mutational status				
KRAS	12 (46)	9 (50)	9 (35)	10 (29)
EGFR ex20	1 (4)	1 (6)	—	1 (3)
BRAF	1 (4)	—	—	1 (3)

Abbreviations: ADC, adenocarcinoma; ECOG PS, Eastern Cooperative Oncology Group performance status; NOS, not otherwise specified; PPI, proton pump inhibitor; SCC, squamous cell carcinoma; TPS, tumor proportion score.

baseline clinical features, oligoAR patients had a prolonged postprogression survival compared with sysAR (median 20.3 vs. 5.6 months; HR, 0.22; 95% CI, 0.10–0.48; $P < 0.001$; **Fig. 3A**).

No significant differences in postprogression survival according to the best RECIST response (CR/PR vs. SD) and the type of treatment (chemotherapy–IO vs. single-agent IO) within oligoAR and sysAR

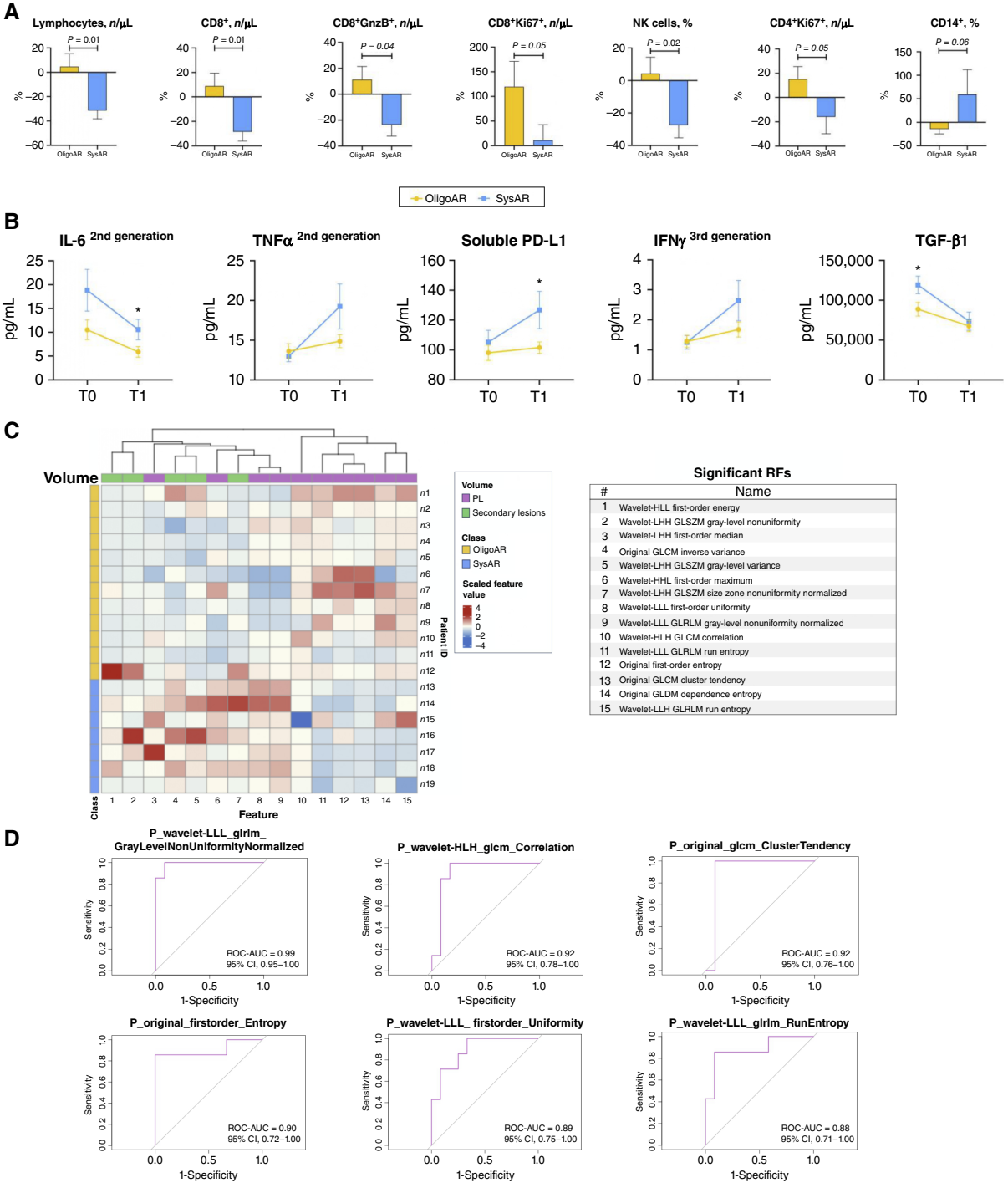

Figure 2.

Radio-immune profile and clinical outcome of oligoAR and sysAR patients. **A,** Representative bar graphs illustrating blood immunophenotypes measured as Δ variation in oligoAR and sysAR patients undergoing ICI-based treatment. *P* values refer to Mann–Whitney test (oligoAR vs. sysAR subsets). **B,** Representative graphs illustrating blood cytokine levels at baseline (T0) and the first disease assessment (T1) in oligoAR and sysAR patients. *, *P* values <0.05 based on Wilcoxon rank sum test (oligoAR vs. sysAR subsets) at T0 and T1, respectively. **C,** Heatmap depicting RFs statistically different between oligoAR and sysAR patients at Δ analysis. The color of each cell indicates the value of individual features (column), scaled using *Z*-score, in any given patient (row); the name of each feature is reported in the table. The top annotation on the heatmap shows the volume of origin of each feature, whereas the annotation on the left indicates the two designated classes of AR on each sample (color legend in the box on the right). **D,** ROC-AUC curves showing the performance of each of the most significant Δ RFs ($P \leq 0.007$ at ROC analysis) in discriminating oligoAR from sysAR. All features were from primary tumors. P, primary tumor; PD, progressive disease.

Table 2. Δ RFs differentially regulated in oligoAR and sysAR.

Δ RFs	OligoAR	SysAR			ROC	
	Median (25th, 75th percentiles)	Median (25th, 75th percentiles)	*P* value*	*P* value**	AUC (95% CI)	*P* value#
P_wavelet-LLL_glrlm_GrayLevelNonUniformityNormalized	**−0.21 (−0.382 to −0.15)**	**0.03 (−0.032 to 0.168)**	**< 0.001**	**0.038**	**0.99 (0.95–1.00)**	**0.001**
P_wavelet-HLH_glcm_Correlation	**0.178 (0.057 to 0.774)**	**−0.572 (−0.659 to −0.368)**	**0.001**	**0.012**	**0.92 (0.78–1.00)**	**0.003**
P_original_glcm_ClusterTendency	**0.604 (0.356 to 2.002)**	**−0.386 (−0.489 to −0.281)**	**0.001**	**0.027**	**0.92 (0.76–1.00)**	**0.003**
P_original_firstorder_Entropy	**0.108 (0.041 to 0.31)**	**−0.063 (−0.065 to −0.041)**	**0.002**	**0.027**	**0.90 (0.72–1.00)**	**0.004**
P_wavelet-LLL_ firstorder_Uniformity	**−0.203 (−0.382 to −0.139)**	**−0.015 (−0.086 to 0.154)**	**0.003**	**0.043**	**0.89 (0.75–1.00)**	**0.005**
P_wavelet-LLL_glrlm_RunEntropy	**0.05 (0.041 to 0.109)**	**−0.064 (−0.09 to −0.03)**	**0.005**	**0.028**	**0.88 (0.71–1.00)**	**0.007**
P_original_gldm_DependenceEntropy	0.035 (0.017 to 0.049)	−0.036 (−0.056 to −0.02)	0.035	0.033	0.79 (0.55–1.00)	0.035
P_wavelet-LLH_glrlm_RunEntropy	0.031 (−0.006 to 0.059)	−0.07 (−0.076 to −0.019)	0.035	0.01	0.80 (0.54–1.00)	0.035
P_wavelet-LHH_firstorder_Median	−0.741 (−1.277 to −0.144)	1.478 (0.232 to 5.529)	0.007	0.012	0.87 (0.70–1.00)	0.009
P_wavelet-HHL_firstorder_Maximum	−0.082 (−0.315 to 0.137)	0.569 (0.373 to 0.669)	0.007	0.013	0.87 (0.74–1.00)	0.009
M_original_glcm_InverseVariance	−0.081 (−0.119 to −0.024)	0.119 (0.026 to 0.155)	0.007	0.007	0.87 (0.70–1.00)	0.009
M_wavelet-LHH_glszm_GrayLevelNonUniformity	−0.75 (−0.914 to −0.571)	0.239 (−0.331 to 3.903)	0.028	0.037	0.81 (0.60–1.00)	0.028
M_wavelet-LHH_glszm_GrayLevelVariance	−0.322 (−0.404 to −0.023)	0.237 (−0.093 to 0.673)	0.035	0.009	0.80 (0.60–1.00)	0.035
M_wavelet-LHH_glszm_SizeZoneNonUniformityNormalized	−0.255 (−0.307 to −0.153)	0.26 (−0.082 to 0.365)	0.007	0.011	0.87 (0.74–1.00)	0.009
M_wavelet-HLL_firstorder_Energy	−0.766 (−0.913 to −0.744)	−0.185 (−0.43 to 0.383)	0.009	0.046	0.86 (0.68–1.00)	0.011

Top rated Δ features are bolded. "P" and "M" labels refer to primary and metastatic volume of origin, respectively.
*, *P* values are referred to Mann–Whitney rank sum test; **, *P* values are referred to permutation test; #, *P* values are referred to ROC analysis.

subgroups were observed, although a trend toward prolonged OS was apparent in oligoAR patients displaying CR/PR (Supplementary Fig. S7).

All the patients experiencing sysAR underwent a therapeutic switch, whereas 10/26 (38%) oligoAR patients continued IO-based therapy beyond progression and 16/26 (61%) received multimodality treatment (IO + local therapy; **Fig. 3B**). Local therapy consisted of radiotherapy in 15 (94%) patients mostly delivered to the lung (8/15), followed by lymph nodes (2/15), whereas only one patient underwent surgical resection.

No differences in terms of postprogression survival were observed between patients receiving local therapy and those who continued IO alone, although a trend toward longer OS was observed in the IO + local therapy group (HR, 0.69; 95% CI, 0.23–2.07; P = NS; data not shown). Notably, of 16 oligoAR cases receiving local therapy, 8 (50%) patients continued immunotherapy or surveillance without further disease progression for at least 6 months after oligoAR development (**Fig. 3B**). Detailed information related to the clinical course of each oligoAR and sysAR patient are graphically reported in **Fig. 3C**.

Site-specific immunophenotypic profile of oligoAR lesions

We further determined whether the number and sites of oligoAR involvement could impact on blood immune parameters. Upon stratification of oligoAR cases (i.e., 1 vs. ≥2 PLs), significantly higher NK cells and $CD8^+Ki67^+$ lymphocytes coupled with lower $CD19^+$ B cells were found to be distinctive baseline features of 1 PL oligoAR cases (**Fig. 4A***i*). Following IO (T1), the PB immune context mirrored baseline features as significantly higher NK cells and lower B cells were detected in 1 PL oligoAR cases, whereas a greater number of Tregs was observed in ≥2 PL oligoAR patients (**Fig. 4Aii**).

OligoAR mostly involved lymph nodes (89%) and lung (80%) metastases, whereas its incidence in bone (31%), pleura (31%), brain (27%), and adrenal gland (4%) was relatively lower. Significantly higher baseline NK cells (P = 0.003) coupled with lower $CD14^+$ monocytes (P = 0.03) and Tregs (P = 0.05) characterized patients displaying lung and lymph nodes compared with bone and brain oligoAR (**Fig. 4Bi**). More distinctive immunophenotypic features emerged at T1 when significantly higher NK cells (P = 0.001) together with an increased fraction of $CD8^+$ (P = 0.05) and $CD4^+$ (P = 0.04) lymphocytes expressing GnzB were present in PB from cases with lung and lymph node oligoAR compared with bone and brain (**Fig. 4Bii**).

We further examined postprogression survival within these oligoAR subgroups (**Fig. 4C**i), documenting a significantly longer OS in patients with 1 compared with 2 to 3 PLs (median NR vs. 12.2 months; HR, 3.21, 95% CI, 1.02–10.14; P = 0.03).

A trend toward a longer OS was observed in patients exhibiting oligoAR at lung and lymph nodes compared with pooled bone/brain sites; however, this difference was not statistically significant (**Fig. 4Cii**).

Discussion

Despite groundbreaking results obtained from IO, it soon became apparent that only a fraction of patients can achieve significant and long-lasting benefits. Heterogeneity in disease response, including dissociation among sites of involvement, also emerged (9, 10, 28). Thus, the observation that AR following initial response to IO might occur asynchronously in primary and metastatic sites, as within different tumor locations, is increasingly receiving attention due to important therapeutic implications. However, the mechanistic insights of this common event in the era of immunotherapy remain largely elusive. Recent attempts to subclassify AR into oligoAR and sysAR just paved the way to really dissect the underlying clinical and immunobiologic cues (15). The interrogation of cancer and immune cells in multiple dimensions might be pursued to unveil the contribution of various factors implicated in the development of specific AR subsets. To this end, a longitudinal approach was undertaken in this study to provide evidence that oligoAR

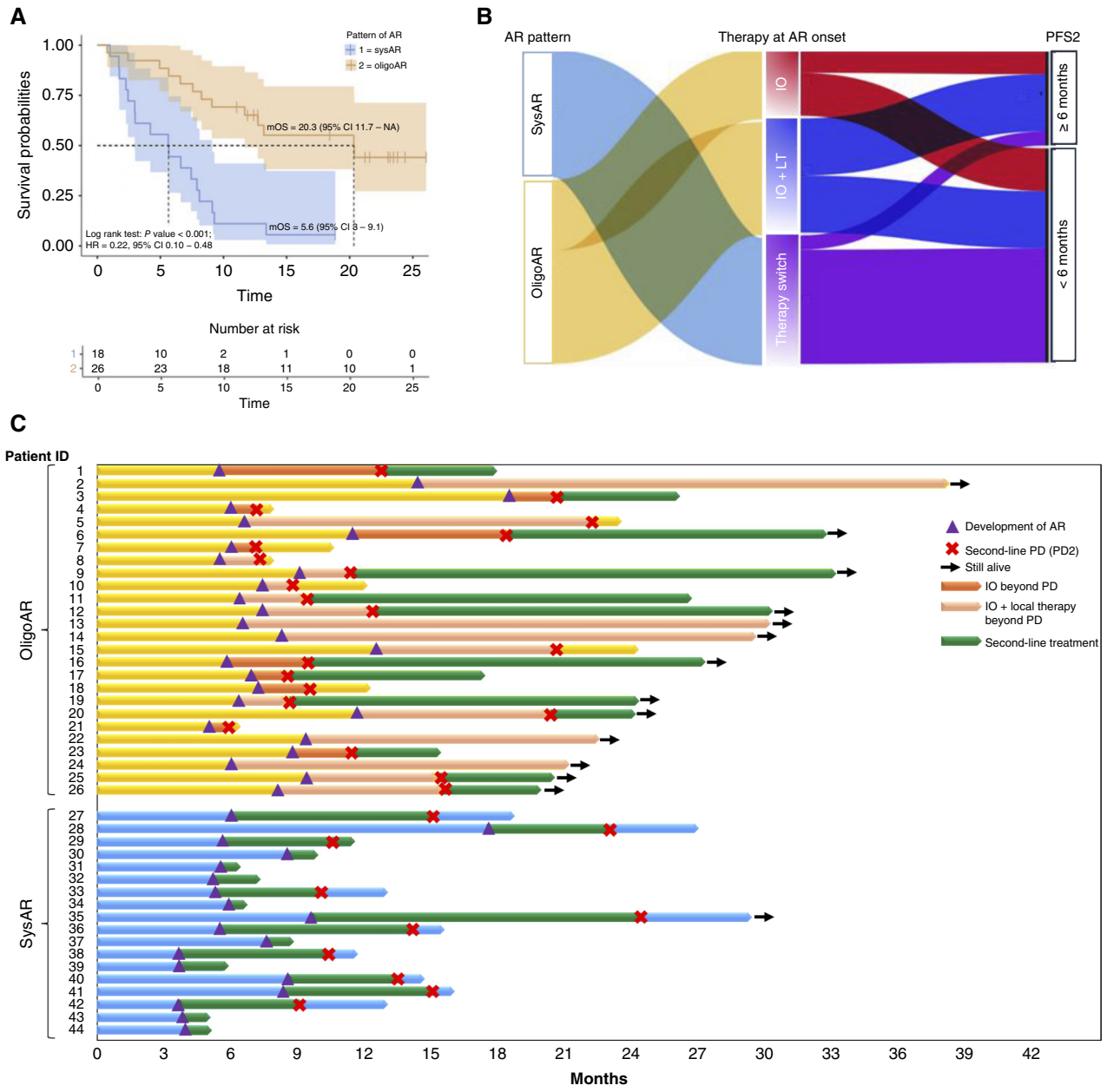

Figure 3.

Clinical outcome of oligoAR and sysAR patients with NSCLC. **A,** Kaplan–Meier curve depicting the postprogression survival outcome (mOS, months) in oligoAR and sysAR patients. Statistical values are inscribed. Number at risk is reported at the bottom of the curve. **B,** Alluvial diagram illustrating the postprogression management of sysAR and oligoAR patients. AR pattern: sysAR (light blue) and oligoAR (yellow); therapy at AR onset: red = IO beyond progression, dark blue = IO + local therapy, and purple = therapeutic switch; PFS2 duration: top = PFS2 ≥6 months, and bottom = PFS2 <6 months. **C,** The clinical course and therapeutic management of each patient developing oligoAR and sysAR are reported in the corresponding swimmer plot. mOS, median OS.

and sysAR to IO in advanced NSCLC recognize distinctive circulating immune-inflammatory features and RFs likely conditioning the different clinical outcomes.

In line with the literature (15), meaningfully prolonged survival outcomes characterized the oligoAR subset, and postprogression management mainly consisted of local therapy, which, at variance, did not exhibit significant prognostic impact. Despite the monocentric nature (single-center study) and the relatively small sample size, potentially attenuating our conclusive remarks, the prospective design, the patient characteristics, which are in line with the literature, the extensive multiparametric readouts and the adequate patient follow-up allowed us to obtain robust findings. Our results support the contention that the timely assessed dynamic of radio-immune parameters might noninvasively discriminate the occurrence of different patterns of IO resistance.

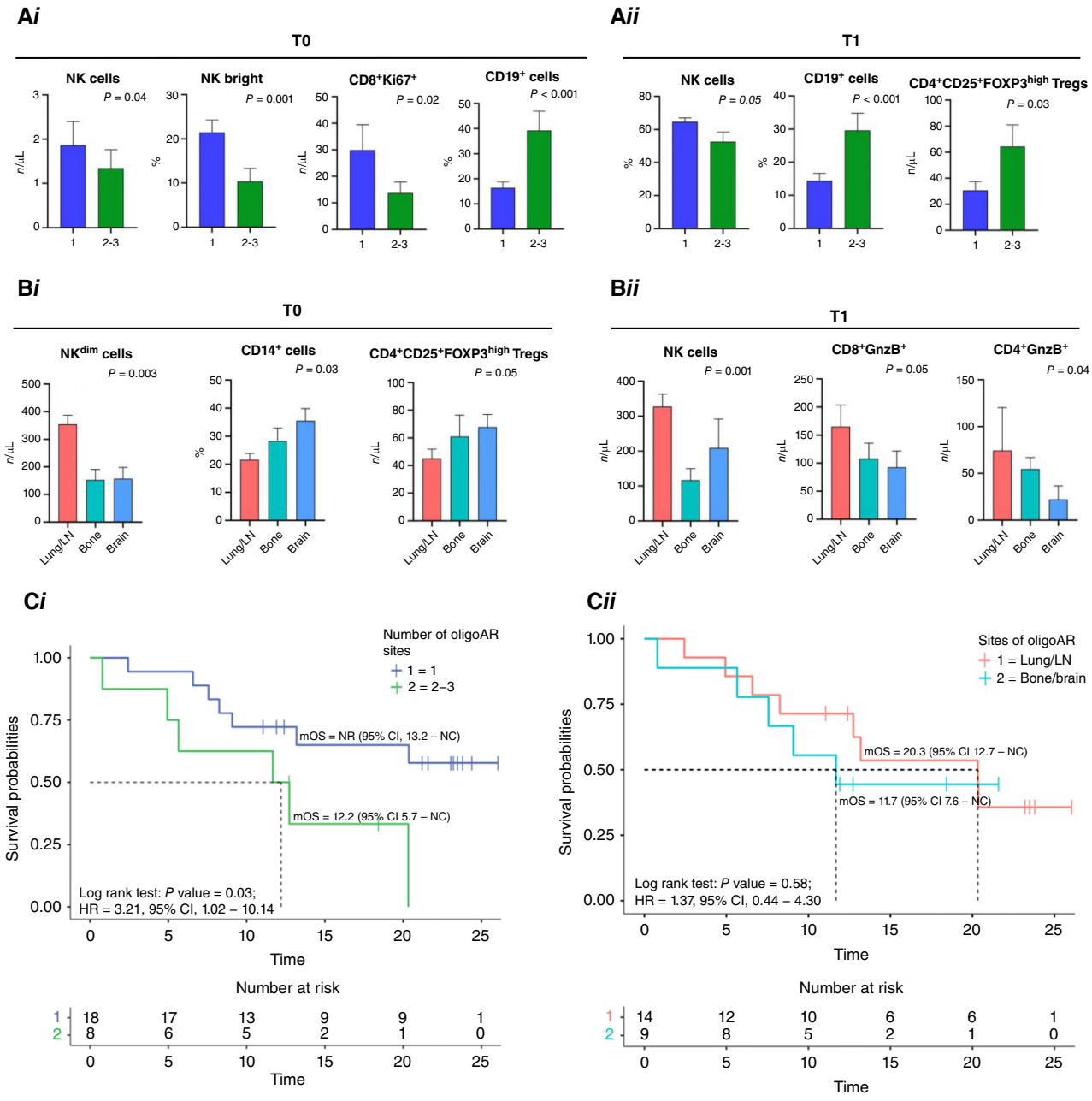

Figure 4.

Blood immunophenotypes and survival outcome according to the number and site of oligoAR. Bar graphs of the distribution of circulating immune cells measured at baseline (T0; **Ai**, **Bi**) and the first disease assessment (**Aii**, **Bii**) according to number (**A**) and anatomic sites (**B**) of oligoAR involvement. **C,** Kaplan–Meier curves illustrating the differential impact on postprogression survival outcome of the number (**Ci**) and pooled lung + lymph node and bone + brain sites (**Cii**) of oligoAR involvement. mOS, months and statistical values are inscribed. Number at risk is reported below the curve. LN, lymph node; mOS, median OS; NC, not calculable.

Tumor-intrinsic and -extrinsic events might contribute to AR, including tumor mutational (29, 30) and neoantigen (31, 32) burden, clonal heterogeneity (33, 34), asynchronous local evasion to antitumor immunity among tumor sites (28, 35, 36), antibody pharmacodynamics and clearance (37), or altered tumor microenvironment–sensitizing IFNγ pathways (38, 39). Additional relevant factors such as the microbiome (40) and drug-to-drug interference (41) might be mechanistically implicated in resistance to immunotherapy.

Genomic/transcriptional analyses on human tumor samples, corroborated by preclinical mouse models, documented that patients with NSCLC developing AR to IO were characterized by persistent inflammation and dysregulated IFNγ signaling rather than a dormant or desert immune background (42). Genomic and

immunophenotypic profiling on an additional cohort of NSCLC was able to identify AR mutations, namely *STK11*, *B2M*, *APC*, *MTOR*, *KEAP1*, and *JAK1/2*, associated with a reduced extent and unfavorable spatial distribution of tumor-infiltrating lymphocytes as distinctive and exclusive features of cases developing AR to IO and not to chemotherapy or targeted therapy (43). Importantly, both studies converged in highlighting the antigen processing machinery as a critical determinant of IO outcome.

In this study, we tested the potential to discern oligoAR and sysAR through the longitudinal interrogation of circulating cellular and humoral modulators of both cancer–host and primary–metastatic tumor interactions, enclosing the systemic tumor immune environment (44). The dynamics of circulating cytotoxic and immunosuppressive elements within the time interval from starting IO to first disease assessment (9–12 weeks) were able to sharply distinguish the immune response of patients with NSCLC developing oligoAR and sysAR. Specifically, the balanced output of blood $CD8^+GnzB^+Ki67^+$ and NK effector and $CD14^+$ ($PD\text{-}1^+$)-suppressive cell populations following IO represented a distinctive feature of the two AR subsets and may underlie their different survival outcomes. We also noticed that the circulating immune profile of the overall AR population was intermediate between NRs, displaying the lowest cytotoxic and the highest immunosuppressive traits and cases with durable benefit (LT-NP) which exhibited both at T0 and T1 prominent lymphocyte activation together with the lowest extent of immune suppressive cells. Overall, these observations are in line with the view that a selected fraction of patients resistant to IO still preserves an efficient antitumor immune response potentially exploitable for tailored therapeutic options.

Before any speculation on the potential link of our cytokine profiling with specific patterns of AR, the short half-life and feedback regulatory mechanisms of these circulating molecules impose some caution in the interpretation of monocentric studies. Our results on IL-6, TNFα, and TGF-β1 levels are in keeping with the more aggressive nature of NSCLC developing sysAR compared with oligoAR and support the proinflammatory background characterizing AR, as recently documented (42). Interestingly, a more robust TGF-β1 inhibition following IO was seen in sysAR, although the significance of this finding is clouded by the dual immunosuppressive and immunostimulatory properties of this cytokine (45) and the influence on its bioavailability by several factors, including stromal remodeling induced by treatment (46).

The potential of radiomics to provide prognostic and predictive biomarkers in IO-treated patients with NSCLC has been repeatedly suggested (21, 22). In the present investigation, Δ RFs extracted from the primary tumor or from a "metastatic volume," derived by merging all secondary lesions, highly performed in discriminating patients developing oligoAR or sysAR. Indeed, the most significant features, all derived from the primary tumors, showed ROC-AUC values between 0.88 and 0.99. Selected studies hypothesized that a radiologic examination of the temporal and spatial patterns of IO response at the level of individual metastases could provide insights into the different contributions of systemic and local features to the antitumor immune response (28). To counter data variability while still preserving a holistic view of patient disease, a smaller but more homogeneous population, carrying both primary and secondary lesions, was selected in this study for radiomic analyses to provide a robust comparison. This analytical step may imply some selection bias because lesions outside the considered acquisition volume were excluded. However, most excluded lesions were brain metastases, which are anyhow difficult to be dynamically assessed MRI being the gold standard for follow-up. The better performance of Δ features in discriminating oligoAR and sysAR patients is supported by previous studies suggesting an improved value of AI models based on the integration of multiple time points (47–49). Differences between groups were also observed at T0, underlining their ability to offer early prognostic information with treatment choice implications. Of note, most of the significantly different T0 and Δ features between the two populations were mainly descriptors of tumor texture and heterogeneity, a frequently reported finding associated with response to IO (21, 23, 50). Although still exploratory, these results show a promising role of radiomics in distinguishing the two AR patterns. Further studies are necessary to clinically translate AI- and radiomic- based readouts upon integration with clinicopathologic, genomic, and immune benchmarks. An additional limitation of our radiomic analysis is that not all CTs were acquired using the same scanner and technical parameters. Whereas this may represent a source of variability, it also reflects the daily clinical practice, in which different acquisition protocols are routinely used, thus increasing the transferability of our results. We aimed to reduce the heterogeneity to a minimum when selecting the volumes on which to perform the segmentations. To further assess whether the different acquisition protocols could represent a significant issue in our analyses, we carried out a PCA. The results, albeit on a small sample size, did not show any evident sample clustering by technical parameters suggestive of the presence of bias.

The arrays of response (i.e., pseudo-, hyper-, and oligo-progression) and the almost inevitable occurrence of AR to IO represent the expression of intra- and inter-tumor heterogeneity in its spatiotemporal components (9, 12, 14). However, assessing the spatial and temporal heterogeneity and its translation into clinical practice embodies a challenging task to improve patient outcomes in the actual immunotherapy scenario. The observation that AR following initial response to IO might occur asynchronously in primary and metastatic sites, as within different tumor locations, is increasingly receiving attention due to important therapeutic implications. A radiomic lesion-level approach has been successfully documented in the literature, although just scratching the surface of inter- and intra-tumor heterogeneity (24, 25, 28). This radiomic subanalysis was, however, prevented in our cohort by the restrained number of included patients, already downsized by the presence of multiple lesions at different sites.

Limited attention has been paid to tissue-specific immunity and how the immune system of each organ may influence cancer development and treatment. Indeed, the composition and function of intrinsic immunoregulatory assets enclosing immunostat (18) might vary according to anatomic sites, differently affecting the ability to locally unleash the adaptive immune response triggered by checkpoint blockade in those organs. The preliminary findings of the present study on the association of blood baseline immune features and their dynamic with specific sites of oligoAR are in agreement with this contention. Indeed, a greater cytotoxic-to-suppressive balance was observed in patients with NSCLC developing resistance to IO in lung and lymph nodes, whereas a more immunosuppressive-driven circulating profile characterized bone and brain resistant lesions. Intriguingly, a trend toward prolonged survival outcomes was also documented in cases developing oligoAR in lung and lymph nodes. These observations suggest that an extensive characterization of the chemokine/cytokine network involved in the reciprocal cross-talk between tissue and blood at the time of resistance may uncover mechanistic insights with potential therapeutic implications.

Importantly, our group is actively involved in the effort to externally validate the obtained results and develop multiomic signatures integrating genomic and transcriptomic data with radioimmune parameters.

In summary, the balanced output of blood effector and suppressor cells, coupled with a differential cytokine modulation, and well-defined Δ RFs distinctively characterize oligoAR and sysAR patients, potentially underlying their different survival outcomes.

Authors' Disclosures

A. Leonetti reports personal fees from AstraZeneca, Bristol Myers Squibb, MSD, Sanofi, Takeda, Novartis, Roche, and Eli Lilly outside the submitted work. M. Tiseo reports grants and personal fees from AstraZeneca, Boehringer Ingelheim, and Roche; personal fees from Novartis, MSD, Merck, Sanofi, Janssen, Daiichi Sankyo, Pierre Fabre, Pfizer, Eli Lilly, and Bristol Myers Squibb; and personal fees and nonfinancial support from Takeda and Amgen outside the submitted work. N. Sverzellati reports grants from the AIRC (Italian Association for Cancer Research) during the conduct of the study. No disclosures were reported by the other authors.

Authors' Contributions

G. Mazzaschi: Conceptualization, data curation, investigation, writing–original draft, project administration, writing–review and editing. **C. Marrocchio:** Data curation, formal analysis, investigation, methodology, writing–original draft. **L. Moron Dalla Tor:** Data curation, software, formal analysis, methodology, writing–original draft. **L. Leo:** Data curation, software, formal analysis, methodology, writing–original draft. **M. Balbi:** Data curation, methodology, writing–review and editing. **G. Milanese:** Investigation, methodology, writing–review and editing. **G.A.R. Adebanjo:** Data curation, formal analysis, methodology. **B. Lorusso:** Data curation, formal analysis, methodology. **G. Monica:** Resources, formal analysis, methodology. **M. Pluchino:** Resources, formal analysis, methodology. **R. Minari:** Resources, supervision, methodology. **S. D'Agnelli:** Resources, formal analysis, methodology. **E. Cardinale:** Resources, data curation, investigation. **F. Perrone:** Resources, investigation. **P. Bordi:** Resources, investigation. **A. Leonetti:** Resources, investigation, writing–review and editing. **R.E. Ledda:** Resources, supervision. **M. Silva:** Resources, validation. **S. Buti:** Supervision, validation, writing–review and editing. **G. Roti:** Resources, supervision, validation, writing–review and editing. **S. Bettati:** Supervision, writing–review and editing. **F. Quaini:** Data curation, supervision, validation, writing–original draft. **M. Tiseo:** Resources, supervision, funding acquisition, project administration, writing–review and editing. **N. Sverzellati:** Supervision, funding acquisition, project administration, writing–review and editing.

Acknowledgments

This work was funded by the AIRC (Italian Association for Cancer Research) research grant to N. Sverzellati (AIRC IG2019-23606). C. Marrocchio, M. Balbi, and L. Moron Dalla Tor were directly supported by these funds.

Note

Supplementary data for this article are available at Clinical Cancer Research Online (http://clincancerres.aacrjournals.org/).

Received June 21, 2024; revised September 10, 2024; accepted December 11, 2024; published first December 13, 2024.

References

1. Sharma P, Hu-Lieskovan S, Wargo JA, Ribas A. Primary, adaptive, and acquired resistance to cancer immunotherapy. Cell 2017;168:707–23.
2. Haslam A, Prasad V. Estimation of the percentage of US patients with cancer who are eligible for and respond to checkpoint inhibitor immunotherapy drugs. JAMA Netw Open 2019;2:e192535.
3. Yu H, Boyle TA, Zhou C, Rimm DL, Hirsch FR. PD-L1 expression in lung cancer. J Thorac Oncol 2016;11:964–75.
4. Samstein RM, Lee CH, Shoushtari AN, Hellmann MD, Shen R, Janjigian YY, et al. Tumor mutational load predicts survival after immunotherapy across multiple cancer types. Nat Genet 2019;51:202–6.
5. Chowell D, Morris LGT, Grigg CM, Weber JK, Samstein RM, Makarov V, et al. Patient HLA class I genotype influences cancer response to checkpoint blockade immunotherapy. Science 2018;359:582–7.
6. Miao D, Margolis CA, Vokes NI, Liu D, Taylor-Weiner A, Wankowicz SM, et al. Genomic correlates of response to immune checkpoint blockade in microsatellite-stable solid tumors. Nat Genet 2018;50:1271–81.
7. Bruni D, Angell HK, Galon J. The immune contexture and immunoscore in cancer prognosis and therapeutic efficacy. Nat Rev Cancer 2020;20:662–80.
8. Huang AC, Postow MA, Orlowski RJ, Mick R, Bengsch B, Manne S, et al. T-cell invigoration to tumour burden ratio associated with anti-PD-1 response. Nature 2017;545:60–5.
9. Nicoś M, Krawczyk P, Crosetto N, Milanowski J. The role of intratumor heterogeneity in the response of metastatic non-small cell lung cancer to immune checkpoint inhibitors. Front Oncol 2020;10:569202.
10. Topp BG, Thiagarajan K, De Alwis DP, Snyder A, Hellmann MD. Lesion-level heterogeneity of radiologic progression in patients treated with pembrolizumab, Ann Oncol 2021;32:1618–25.
11. Borcoman E, Kanjanapan Y, Champiat S, Kato S, Servois V, Kurzrock R, et al. Novel patterns of response under immunotherapy, Ann Oncol 2019;30:385–96.
12. Tazdait M, Mezquita L, Lahmar J, Ferrara R, Bidault F, Ammari S, et al. Patterns of responses in metastatic NSCLC during PD-1 or PDL-1 inhibitor therapy: comparison of RECIST 1.1, irRECIST and iRECIST criteria. Eur J Cancer 2018;88:38–47.
13. Schoenfeld AJ, Antonia SJ, Awad MM, Felip E, Gainor J, Gettinger SN, et al. Clinical definition of acquired resistance to immunotherapy in patients with metastatic non-small-cell lung cancer, Ann Oncol 2021;32:1597–607.
14. Schoenfeld AJ, Hellmann MD. Acquired resistance to immune checkpoint inhibitors. Cancer Cell 2020;37:443–55.
15. Schoenfeld AJ, Rizvi HA, Memon D, Shaverdian N, Bott MJ, Sauter JL, et al. Systemic and oligo-acquired resistance to PD-(L)1 blockade in lung cancer. Clin Cancer Res 2022;28:3797–803.
16. Syn NL, Teng MWL, Mok TSK, Soo RA. De-novo and acquired resistance to immune checkpoint targeting. Lancet Oncol 2017;18:e731–41.
17. Dagogo-Jack I, Shaw AT. Tumour heterogeneity and resistance to cancer therapies. Nat Rev Clin Oncol 2018;15:81–94.
18. Pao W, Ooi CH, Birzele F, Ruefli-Brasse A, Cannarile MA, Reis B, et al. Tissue-specific immunoregulation: a call for better understanding of the "immunostat" in the context of cancer. Cancer Discov 2018;8:395–402.
19. Sade-Feldman M, Yizhak K, Bjorgaard SL, Ray JP, de Boer CG, Jenkins RW, et al. Defining T cell states associated with response to checkpoint immunotherapy in melanoma. Cell 2018;175:998–1013.e20.
20. Yost KE, Satpathy AT, Wells DK, Qi Y, Wang C, Kageyama R, et al. Clonal replacement of tumor-specific T cells following PD-1 blockade. Nat Med 2019;25:1251–9.
21. Roisman LC, Kian W, Anoze A, Fuchs V, Spector M, Steiner R, et al. Radiological artificial intelligence—predicting personalized immunotherapy outcomes in lung cancer. NPJ Precis Oncol 2023:7:125.
22. Chen M, Copley SJ, Viola P, Lu H, Aboagye EO. Radiomics and artificial intelligence for precision medicine in lung cancer treatment. Semin Cancer Biol 2023;93:97–113.
23. Ladbury C, Amini A, Govindarajan A, Mambetsariev I, Raz DJ, Massarelli E, et al. Integration of artificial intelligence in lung cancer: rise of the machine. Cell Rep Med 2023;4:100933.
24. Henry T, Sun R, Lerousseau M, Estienne T, Robert C, Besse B, et al. Investigation of radiomics based intra-patient inter-tumor heterogeneity and the impact of tumor subsampling strategies. Sci Rep 2022;12:17244.
25. Song C, Park H, Lee HY, Lee S, Ahn JH, Lee SH. Evaluation of response to immune checkpoint inhibitors using a radiomics, lesion-level approach. Cancers (Basel) 2021;13:6050.
26. Mazzaschi G, Facchinetti F, Missale G, Canetti D, Madeddu D, Zecca A, et al. The circulating pool of functionally competent NK and $CD8^+$ cells predicts the outcome of anti-PD1 treatment in advanced NSCLC. Lung Cancer 2019;127:153–63.

27. Mezquita L, Auclin E, Ferrara R, Charrier M, Remon J, Planchard D, et al. Association of the lung immune prognostic index with immune checkpoint inhibitor outcomes in patients with advanced non-small cell lung cancer. JAMA Oncol 2018;4:351–7.
28. Osorio JC, Arbour KC, Le DT, Durham JN, Plodkowski AJ, Halpenny DF, et al. Lesion-level response dynamics to programmed cell death protein (PD-1) blockade. J Clin Oncol 2019;37:3546–55.
29. Zaretsky JM, Garcia-Diaz A, Shin DS, Escuin-Ordinas H, Hugo W, Hu-Lieskovan S, et al. Mutations associated with acquired resistance to PD-1 blockade in melanoma. N Engl J Med 2016;375:819–29.
30. Vryza P, Fischer T, Mistakidi E, Zaravinos A. Tumor mutation burden in the prognosis and response of lung cancer patients to immune-checkpoint inhibition therapies. Transl Oncol 2023;38:101788.
31. Sade-Feldman M, Jiao YJ, Chen JH, Rooney MS, Barzily-Rokni M, Eliane JP, et al. Resistance to checkpoint blockade therapy through inactivation of antigen presentation. Nat Commun 2017;8:1136.
32. Gettinger S, Choi J, Hastings K, Truini A, Datar I, Sowell R, et al. Impaired HLA class I antigen processing and presentation as a mechanism of acquired resistance to immune checkpoint inhibitors in lung cancer. Cancer Discov 2017;7:1420–35.
33. Nowell PC. The clonal evolution of tumor cell populations. Science 1976;194:23–8.
34. Jamal-Hanjani M, Wilson GA, McGranahan N, Birkbak NJ, Watkins TBK, Veeriah S, et al. Tracking the evolution of non-small-cell lung cancer. N Engl J Med 2017;376:2109–21.
35. Hu Z, Li Z, Ma Z, Curtis C. Multi-cancer analysis of clonality and the timing of systemic spread in paired primary tumors and metastases. Nat Genet 2020;52:701–8.
36. Guan Y, Feng D, Yin B, Li K, Wang J. Immune-related dissociated response as a specific atypical response pattern in solid tumors with immune checkpoint blockade. Ther Adv Med Oncol 2022;14:17588359221096877.
37. Guo Y, Remaily BC, Thomas J, Kim K, Kulp SK, Mace TA, et al. Antibody drug clearance: an underexplored marker of outcomes with checkpoint inhibitors. Clin Cancer Res 2024;30:942–58.
38. Gao J, Shi LZ, Zhao H, Chen J, Xiong L, He Q, et al. Loss of IFN-γ pathway genes in tumor cells as a mechanism of resistance to anti-CTLA-4 therapy. Cell 2016;167:397–404.e9.
39. Chen PL, Roh W, Reuben A, Cooper ZA, Spencer CN, Prieto PA, et al. Analysis of immune signatures in longitudinal tumor samples yields insight into biomarkers of response and mechanisms of resistance to immune checkpoint blockade. Cancer Discov 2016;6:827–37.
40. Routy B, Le Chatelier E, Derosa L, Duong CPM, Alou MT, Daillère R, et al. Gut microbiome influences efficacy of PD-1-based immunotherapy against epithelial tumors. Science 2018;359:91–7.
41. Cortellini A, Tucci M, Adamo V, Stucci LS, Russo A, Tanda ET, et al. Integrated analysis of concomitant medications and oncological outcomes from PD-1/PD-L1 checkpoint inhibitors in clinical practice. J Immunother Cancer 2020;8:e001361.
42. Memon D, Schoenfeld AJ, Ye D, Fromm G, Rizvi H, Zhang X, et al. Clinical and molecular features of acquired resistance to immunotherapy in non-small cell lung cancer. Cancer Cell 2024;42:209–24.e9.
43. Ricciuti B, Lamberti G, Puchala SR, Mahadevan NR, Lin J-R, Alessi J V, et al. Genomic and immunophenotypic landscape of acquired resistance to PD-(L)1 blockade in non-small-cell lung cancer. J Clin Oncol 2024;42:1311–21.
44. Xu L, Zou C, Zhang S, Chu TSM, Zhang Y, Chen W, et al. Reshaping the systemic tumor immune environment (STIE) and tumor immune microenvironment (TIME) to enhance immunotherapy efficacy in solid tumors. J Hematol Oncol 2022;15:87.
45. Principe DR, Doll JA, Bauer J, Jung B, Munshi HG, Bartholin L, et al. TGF-β: duality of function between tumor prevention and carcinogenesis. J Natl Cancer Inst 2014;106:djt369.
46. Metropulos AE, Munshi HG, Principe DR. The difficulty in translating the preclinical success of combined TGFβ and immune checkpoint inhibition to clinical trial. eBioMedicine 2022;86:104380.
47. Khorrami M, Prasanna P, Gupta A, Patil P, Velu PD, Thawani R, et al. Changes in CT radiomic features associated with lymphocyte distribution predict overall survival and response to immunotherapy in non-small cell lung cancer. Cancer Immunol Res 2020;8:108–19.
48. Barabino E, Rossi G, Pamparino S, Fiannacca M, Caprioli S, Fedeli A, et al. Exploring response to immunotherapy in non-small cell lung cancer using delta-radiomics. Cancers (Basel) 2022;14:350.
49. Cousin F, Louis T, Dheur S, Aboubakar F, Ghaye B, Occhipinti M, et al. Radiomics and delta-radiomics signatures to predict response and survival in patients with non-small-cell lung cancer treated with immune checkpoint inhibitors. Cancers 2023;15:1968.
50. Saad MB, Hong L, Aminu M, Vokes NI, Chen P, Salehjahromi M, et al. Predicting benefit from immune checkpoint inhibitors in patients with non-small-cell lung cancer by CT-based ensemble deep learning: a retrospective study. Lancet Digit Health 2023;5:e404–20.